Analysis of the horizontal momentum budget in the surface layer at Cabauw

(U.S. Department of Energy, 2015)

By

Gijs van Ouwerkerk

Supervisors
Dr. S. R. de Roode
Prof. Dr. H. Jonker

Abstract

In this research, a momentum budget analysis is conducted to quantify the contributions of its various components. The analysis is based on wind velocity and air pressure data of 48 KNMI measurement stations in a 100-km radius of Cabauw in the Netherlands, over the period July 2016 to May 2018. It is found that the Coriolis term in the momentum balance has a magnitude of only a third of the pressure term, which deviates strongly from the geostrophic balance. The imbalance between pressure and Coriolis is countered by turbulence, which has the same order of magnitude as the pressure term and acts as a damping force to flow acceleration. Analysis shows that turbulent fluxes vary linearly with wind velocity and a coefficient for this relation can be quantified. In addition, the diurnal trends in the momentum balance and especially of turbulence is diagnosed for a period of stable, clear sky weather. The results herein show that turbulent fluxes are stronger and have a larger variance during day-time compared to night-time.

Acknowledgements

This thesis has been written as a final project for the bachelor study Applied Earth Sciences at the TU Delft. The subject is part of the department of Geoscience & Remote Sensing at the facility of Civil Engineering and Geosciences of the TU Delft. This project is done in order to get a better understanding of the complete atmospheric momentum budget based on observation data. I would like to offer my special thanks to my supervisor Dr. S. R. de Roode for all the help, insights and discussions needed to complete this project. Also, I would like to thank my second supervisor Prof. Dr. H. Jonker of the weather forecast and simulation company Whiffle for the help and data needed to complete my research. Finally, I would like to express my appreciation to Pim van Dorp of Whiffle, for the initial processing and preparation of the data sets.

Nomenclature

ABL	Atmospheric Boundary Layer
CESAR	Cabauw Experimental Site for Atmospheric Research
DALES	Dutch Atmospheric Large-Eddy Simulation
GALES	GPU-resident Atmospheric Large-Eddy Simulation
GCM	Global Climate Model
KNMI	Royal Netherlands Meteorological Institute
LES	Large-Eddy Simulation
PDF	Probability Density Function
RACMO	Regional Atmospheric Climate Model
RCM	Regional Climate Model

Table of Contents

List of Figures

List of Tables

Chapter 1: Introduction

Wind powered energy has established itself as an important alternative to carbon based electricity generation. Wind turbines provide a source of practically inexhaustible power generation, yet progress in technology and weather forecasting models are still needed in order for wind energy to take up a larger part of the energy matrix. As wind power lacks the uniformity of fossil fuel based power generation, wind power forecasting is of vital importance for further integration of windfarms in our current energy system. The challenge of wind energy for the current system is comprehensive grid balancing, which is the matching of energy supply and demand by the grid managers. This task has become more unpredictable and expensive by constraint payments made to electricity suppliers to shutdown wind farms in times of overproduction or to conventional generator in times of shortages. In the Netherlands, electricity is traded on the Day-Ahead market at the Amsterdam Power Exchange (Apxgroup.com, 2018). On the Day-Ahead market, producers and customers trade one day in advance of the delivery of electricity. Trade members submit their orders electronically, where after supply and demand are compared and a market price is set for each hour of the following day (Apxgroup.com, 2018). On the day itself, small corrections take place on the 15-minute spot market. Together with innovative energy storage techniques, more accurate and spatially detailed weather predictions can provide a better tool for comprehensive grid management, trading information and power generation.

Short, middle and long-term atmospheric models present an inside in weather and wind behaviour. The models are based on a collection of primitive equations, and approximate the future state of the atmosphere by analysing the rates of change and applying them to the previous modelled state (Qian, 2017). Numerical methods are used to approximate solutions for the nonlinear partial differential primitive equations describing the rate of change of state of the atmosphere in the model. Atmospheric models come in different domains: global models covering the entire Earth known as Numerical Weather Prediction (NWP) Model, and regional models covering only a section of the atmosphere known as Limited Area Weather Model (LAM). The difference in model domain is reflected in the solution method: NWP models make use of spectral methods in the horizontal range and finite difference methods for the vertical range, whereas regional coverage LAM only uses three-dimensional finite-difference methods (Strikwerda, 2004). LAMs have a finer grid size by which they are more precise and able to analyse smaller scale atmospheric changes. Due to the high computational demand of this method and grid size, the model can only be applied regionally. The boundary and initial conditions of the regional models are based on compatible global models, the uncertainties and errors of those carry on into the LAM.

1.1 Modelling Methods

The state of the Atmospheric Boundary Layer (ABL) can be model with a Large-Eddy Simulation (LES). With this technique turbulent flows are modelled by solving for space- and time-averaged versions of the governing Navier-Stokes equation. To reduce computational cost LES ignores the smallest length scales by applying low-pass filtering of the Navier-Stokes equation (Valero-Lara, 2018). This filtering can be seen as taking time- and spatial-averaging in order to dismiss the smallest scale information from the numerical solution. An even higher resolution can be accomplished by Direct Numerical Simulation (DNS), but this requires large computational power and is therefore expensive and only applied on a very small domain (Kurien and Taylor, 2005).

The Regional Atmospheric Climate Model (RACMO) is a LAM model used for short term weather and wind speed forecasting. RACMO is a regional climate model (RCM) developed by the Royal Netherlands Meteorological Institute (KNMI) in corporation with the Danish Meteorological Institute. RCM's are more and more used for downscaling global climate models (GCM) to improve special and temporal resolutions. However, small-scale (5 – 10 km) features prove to be a challenge for RCM's (van der Hurk, van Meijgaard & Lenderink, 2018). Dutch Atmospheric Large-Eddy Simulation (DALES) is a CPU resident LES model. GPU-resident Atmospheric Large-Eddy Simulation (GALES) is a LES model that completely runs on an GPU-card (Schalkwijk et al., 2015). This allows for simulation on a large domain at high resolution for short term weather and wind forecasting. An LES data set that is used later in this paper is presented by Schalkwijk (2015), which is run on input of the regional climate model RACMO for a 25x25km domain with a resolution of 25m over the site of the Cabauw measurement station. The KNMI-mast Cabauw is a 213-high meteorological measurement station with measurement equipment at selected elevations (Knmi.nl, 2018).

Chapter 2: Research question

The introduction of LES models, such as GALES, have significantly improved the spatial resolution to which the atmospheric boundary layer can be analysed and its future state can be modelled. A snapshot of the North-South component of the wind velocity during a cold air outbreak wind as obtained from UCLA-LES is presented in (Figure 1). This snapshot shows the fluctuations in wind velocity with respect to the horizontal average ($v_{avg} \pm -15$ m/s). Interestingly are the significant wind velocity gradient and structures on a small 1 to 10 km range. These structures can arise in any case of atmospheric instability and turbulence. This observation shows that wind velocity varies strongly in time at a fixed point in space, as structures with high flow gradients pass by.

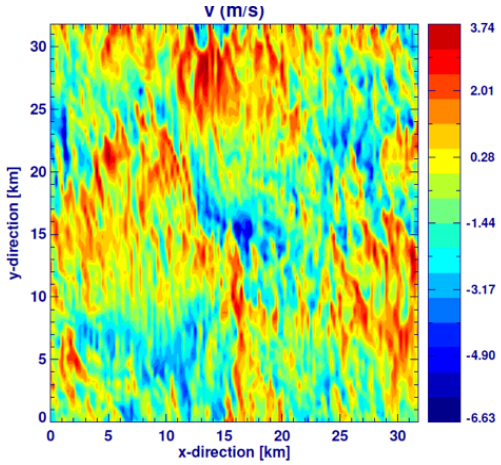

Figure 1: Contour plots of absolute deviation of wind velocity component u and v at 100m elevation by UCLA-LES run for cold air outbreak case (de Roode et al., n.d.)

The total acceleration of the atmospheric flow field can be defined as Eq. (2.1). Other forces and physical quantities of influence to flow acceleration will be discussed in chapter 3.

$$\underbrace{\frac{Dv}{Dt}}_{total\ acceleration} = \underbrace{\frac{\partial v}{\partial t}}_{local\ acceleration\ term} + \underbrace{u\frac{\partial v}{\partial x} + v\frac{\partial v}{\partial y} + w\frac{\partial v}{\partial z}}_{advective\ acceleration\ terms} \qquad 2.1$$

Holton (1992), suggest that in general the total acceleration of the horizontal flow field ($\frac{Du}{Dt}$ and $\frac{Dv}{Dt}$) is of the order 10^{-4} m/s^2 and that the local acceleration term and advective acceleration terms are of comparable magnitude. Based on (Figure 1) an estimation can be made of the North-South advective acceleration term in the flow field: $v\frac{\partial v}{\partial y} \approx 15\ \frac{10}{10000} = 1.5\ x\ 10^{-2}$ m/s^2. This estimation of the local advective acceleration by the model is significantly higher the suggested advective acceleration magnitude (order 10^{-4} m/s^2) by Holton (1992).

This discrepancy in magnitude between literature based and modelled advective acceleration motivates to look at the magnitude of the local acceleration. The local acceleration component of the wind can be derived from modelled data as well as observations. Local acceleration for the year 2012 over a 25x25 km domain in the Netherlands is analysed based on the following data:

- Cabauw meteorological measurement station
- Large-eddy simulation model: GALES
- Limited Area Weather Model: RACMO

A comparison of the local wind acceleration is made by specifying the probability of the random variable local acceleration $\frac{\partial u}{\partial t}$ for Cabauw and mean local acceleration $\frac{\partial \overline{u}}{\partial t}$ for GALES and RACMO in the year 2012 (Figure 2). In the comparison of the PDFs it is visible that the variation and magnitude of the local mean acceleration term of GALES ($\frac{\partial \overline{u}}{\partial t} \leq 0.5x10^{-3}$ m/s^2) and RACMO ($\frac{\partial \overline{u}}{\partial t} \leq 1.0x10^{-3}$ m/s^2) are significant lower than the local acceleration measurement of Cabauw ($\frac{\partial u}{\partial t} \leq 2.0x10^{-3}$). As the PDFs of the local mean acceleration of GALES and RACMO are an average over the entire 25x25 km domain, the local variability in wind velocity is partly averaged out.

The daily initial and boundary conditions for the GALES model are based on RACMO data, by this diurnal cycle the GALES model is continuously nudged towards the RACMO values. The RACMO PDF of $\frac{\partial \overline{u}}{\partial t}$ compared to the GALES PDF of $\frac{\partial \overline{u}}{\partial t}$ corresponds better to the local acceleration of the Cabauw observations (Figure 2). This indicates that the physical processes resulting in the smaller magnitude and variation in $\frac{\partial \overline{u}}{\partial t}$ in GALES over RACMO happen on a time scale smaller than the nudging time scale. Also, this suggest that the process leading to strong variation in $\frac{\partial \overline{u}}{\partial t}$ might happen on a scale for which RACMO does not have the correct spatial variability.

The RACMO PDF of $\frac{\partial \overline{u}}{\partial t}$ compared to the GALES PDF of $\frac{\partial \overline{u}}{\partial t}$ shows a stronger variability in the local mean acceleration (Figure 2). It is apparent from the discrepancy in $\frac{\partial \overline{u}}{\partial t}$ between GALES and RACMO, that either one or both models insufficiently or incorrectly model the local acceleration term. An analysis of the contribution of the local acceleration term and advection term in the total momentum budget, can give a good indication of the contribution of the terms to the modelled solution. Also, evident form (Figure 2) is that the spread in magnitude of wind acceleration is larger at higher elevations for both observation and model data.

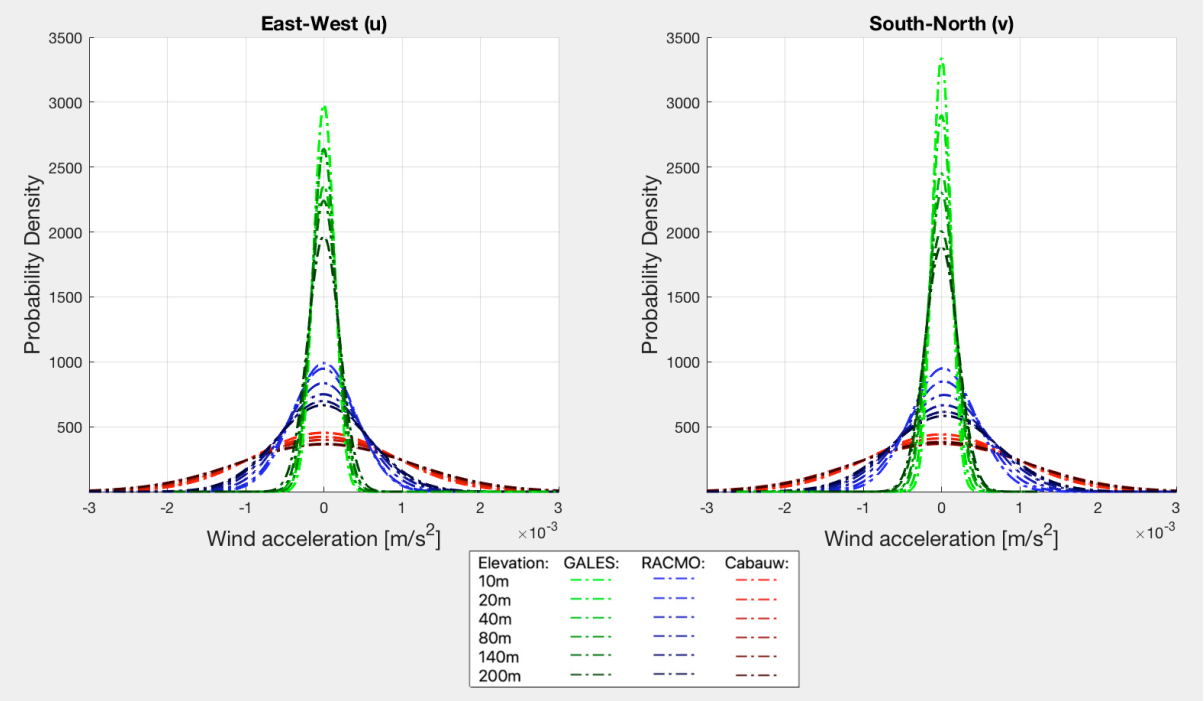

Figure 2: Probability density function of local wind acceleration ($\partial u/\partial t$) on a 1 hour interval for Cabauw observations, and mean local acceleration ($\partial \bar{u}/\partial t$) on a 1 hour interval for RACMO model data and GALES model data. Wind direction component u (East-West) on the left and component v (South-North) on the right.

The difference in the range of local acceleration between observations and modelled data, together with the discrepancy in the magnitude of the advective acceleration, motivates to look at the complete momentum budget driving atmospheric flow. An analysis of the contributions of each term of the total momentum budget, will help to understand and better model the future state of the atmosphere. Therefore, the main aim of this research is: Diagnose the full horizontal momentum budget equation with the use of observation data collected during a period of two year at KNMI weather stations.

Chapter 3: Momentum Balance

3.1 Synoptic-scale modelling

Dynamic meteorology concerns the analysis of the atmosphere and the weather and climate patterns associated with it. The atmosphere can be characterized by various physical quantities such as: density, pressure and temperature. The partial differential equations describing the evolution of the atmospheric physical quantities, and with that the state of the atmosphere, are very complex and no general solution is known (Holton, 1992). Atmospheric motion is governed by the laws of fluid mechanics, gas and thermodynamics and can approximately be described by the three fundamental physical relations of: conservation of energy, conservation of mass, and conservation of momentum. In the most general form the horizontal wind momentum balance is derived in the Lagrangian frame and Cartesian coordinates Eqs. (3.1) and (3.2) (Holton, 1992). The horizontal equations with additional information contained in boundary conditions gives us numerical mathematical tools to describe the motion of the atmosphere, i.e. wind. To get a better understanding of the atmospheric motions and its role on weather and climate, models are based on systematic simplification of the governing equations (Holton, 1992).

$$\underbrace{\frac{\partial u}{\partial t}}_{acceleration\ term} + \underbrace{u\frac{\partial u}{\partial x} + v\frac{\partial u}{\partial y} + w\frac{\partial u}{\partial z}}_{advection\ terms} = \underbrace{fv}_{Coriolis\ term} - \underbrace{\frac{1}{\rho}\frac{\partial p}{\partial x}}_{pressure\ term} + \underbrace{F_{rx}}_{Frictional\ force} \qquad 3.1$$

$$\underbrace{\frac{\partial v}{\partial t}}_{acceleration\ term} + \underbrace{u\frac{\partial v}{\partial x} + v\frac{\partial v}{\partial y} + w\frac{\partial v}{\partial z}}_{advection\ terms} = \underbrace{-fu}_{Coriolis\ term} - \underbrace{\frac{1}{\rho}\frac{\partial p}{\partial y}}_{pressure\ term} + \underbrace{F_{ry}}_{Frictional\ force} \qquad 3.2$$

In the horizontal momentum balance Eqs. (3.1) and (3.2), u is the zonal wind component (East-West), v is the meridional wind component (South-North) and w is the vertical element of the wind. Furthermore, p represents the pressure and the derivative its horizontal gradient, ρ is the density of the air, dependent upon the local pressure and temperature and F is the molecular friction force. The Coriolis frequency f Eq. (3.3) is dependent upon the rotation rate of the earth (Ω) and the latitude of the position of consideration (φ)

$$f = 2\Omega\, sin\varphi \qquad 3.3$$

The total LHS of the momentum balance represents the expansion of the total velocity derivative $\frac{Du}{Dt}$ and $\frac{Dv}{Dt}$ of the 3-dimensional flow field, composed of the local acceleration term and advection terms. The decomposition Eq. (2.1) into the two acceleration terms follows from the chain rule of differentiation. The pressure gradient term describes the difference in air pressure between two arbitrary points on the earth's surface or in the atmosphere. The pressure difference is a main driving force of the wind motion, striving to balance out the variation in pressure.

3.2 Scale analysis by Holton (1992)

To estimate the magnitude of the various terms in the momentum balance a scale analysis can be performed. In this analysis, typical magnitudes and amplitudes of the physical quantities are stated. These quantities are then used to determine the contributions of each term to the governing equations, Eqs. (3.1) and (3.2). If a term is of negligible magnitude, it might be valid to eliminate it from the equation, hence further simplifying models for atmospheric motion. One such scaling analysis is performed by James R. Holton in 'An Introduction to Dynamic Meteorology'. Holton (1992) describes characteristic scales of variables for synoptic-scale motions in mid-latitude systems (Table 1).

Table 1: Characteristic scales of field variables (Holton, 1992).

U	10 [m/s]	Horizontal velocity scale
W	1 [cm/s]	Vertical velocity scale
L	10^6 [m]	Length scale
H	10^4 [m]	Depth scale
$\delta P/\rho$	10^3 [m/s^2]	Horizontal pressure fluctuation scale
L/U	10^5 [s]	Time scale

It is not possible to consider the synoptic-scale vertical velocity directly in this analysis (Holton, 1992). However, the magnitude of the horizontal velocity is several times larger than that of the vertical velocity and therefore the vertical velocity is not considered to be of significant importance (Mesoscale Research Group, 2014). The magnitude of each term in the governing horizontal equations, Eqs. (3.1) and (3.2) are given in (Table 2) for a latitude of 45°. In the scale analysis Holton (1992) considers the free troposphere, hence leaving a magnitude analysis of turbulence.

Table 2: Scale analysis of the horizontal (x-direction, y-direction) momentum balance equations (Holton, 1992).

X-equation	$\frac{Du}{Dt}$	fv	$\frac{1}{\rho_0}\frac{\partial p}{\partial x}$	F_{rx}
Y-equation	$\frac{Dv}{Dt}$	fu	$\frac{1}{\rho_0}\frac{\partial p}{\partial y}$	F_{ry}
Scales	$\frac{U^2}{L}$	$f_0 U$	$\frac{\partial P}{\rho L}$	$\frac{\nu U}{H^2}$
[m/s^2]	10^{-4}	10^{-3}	10^{-3}	10^{-12}

From Table 2 it is obvious that molecular friction is negligible for synoptic-scale motions, only near the surface at the smallest scale turbulent motion it must be considered (Holton, 1992). It is also apparent from Table 2 that the Coriolis and Pressure term are of the same magnitude. The pressure term together with the Coriolis term and friction influences the wind direction. The Rossby Eq. (3.4) number is a non-dimensional measure of the magnitude of the wind acceleration, compared to the Coriolis force. For synoptic scale weather systems, the characteristic length scale L is large, resulting in a small Rossby number. The smaller the Rossby number, the better the geostrophic balance can be used. The Reynolds number Eq. (3.5) is a non-dimensional measure of the friction effect with respect to the inertial term. For low Reynolds number, i.e. Re<1, friction forces dominate and for large Reynolds number, i.e. Re>>1 friction can be neglected. In case of atmospheric winds, it is valid to consider a small Rossby number and large Reynolds number (J. H. LaCasce, 2008).

$$Ro = \frac{u}{Lf} \quad 3.4$$

$$Re = \frac{uL}{\nu} \quad 3.5$$

For a Coriolis parameter of f ~ 10^{-4}, an atmospheric flow of u ~ 10 m/s with a length scale of ~ 1000km (scale of low/high pressure systems) and laminar kinematic viscosity of $\nu \sim 0.01\ x\ 10^{-4}$ m/s^2, Ro ~ 0.1 and Re>>1. This numerical example shows that for characteristic atmospheric magnitude, neglecting molecular friction is valid and that the entire pressure gradient balances the Coriolis force (USNA, n.d.). So, in a spatially varying pressure field under steady-state flow, the Coriolis term and pressure term are presumably in geostrophic balance. The balance implies that when the pressure gradient is known, the wind velocity can be approximately described according to the Geostrophic Flow Equation (3.6) (Mesoscale Research Group, 2014). This is under the assumption that the acceleration of the 3-dimensional flow field is equal to zero and other force can be neglected. This approximation Eq. (3.6) has no dependency on time anymore, therefore it cannot be used for a prediction of the evolution of the flow field (Holton, 1992).

$$V_{geo} = \frac{1}{\rho f}\frac{\partial p}{\partial x} \qquad U_{geo} = -\frac{1}{\rho f}\frac{\partial p}{\partial y} \quad 3.6$$

For synoptic-scale a pressure system, the geostrophic balance implies that the flow field is parallel along the isobars, and that the pressure is constant along the streamlines of the flow field. A larger gradient results in a faster wind flow in the direction form the high-pressure region to the low-pressure region. However, as can be derived from the momentum equations, winds do not travel along straight lines, due to the rotation of the Earth. The Coriolis Effect is a force acting on moving objects, deflecting them out of their path in respect to the earth surface. Flow is counter clockwise for low pressure systems and clockwise for high pressure systems in the northern hemisphere Eq. (3.6).

To predict the evolution of the synoptic-scale flow field the total acceleration ($\frac{Du}{Dt}\ and\ \frac{Dv}{Dt}$) need to be considered. The often-used approximate horizontal momentum is then composed of the total acceleration and geostrophic balance (Holton, 1992). The total acceleration terms ($\frac{Du}{Dt}$, $\frac{Dv}{Dt}$) are proportional to the difference between the geostrophic wind and actual wind (Holton, 1992). According to Holton (1992) this implies that the acceleration terms are of one magnitude smaller than the pressure term and Coriolis term, which is in accordance with the performed scale analysis (Table 2).

3.3 Atmospheric boundary layer modelling

In the atmospheric boundary layer (ABL) the atmospheric flow field is altered as it interacts the with planet's surface resulting in turbulent motion and transport. For the approximation of synoptic-scale motions in the free atmosphere (above the turbulent layer), the turbulent motions may be ignored (Holton, 1992). However, in case of the ABL turbulence needs to be considered in the momentum balance, as the transport of momentum through turbulent eddies strongly alters the momentum balance.

The ABL is often divided into three vertical zones. The lowest zone considers only the first few centimetres of the atmosphere. For this layer flow can be considered laminar, but its thickness makes it irrelevant for the applications of this research. The second zone, known as the constant flux layer or Prandtl layer, makes up the next roughly 100 meters. In this zone, turbulent forces play a significant role on the wind speed (Emeis, 2013). The last zone of the ABL is known as the Ekman layer and ranges from 100 meters in depth at night to 2-3 km in depth during sunny days (Emeis, 2013). As identified in the scale analysis by Holton (1992), the pressure term and Coriolis term in the momentum balance are of most importance synoptic-scale motions. According to Emeis (2013), the weight distribution of the terms in the momentum balance is different for the various zones in the ABL. In the Prandtl layer an equilibrium can be observed between the pressure term and the frictional forces induced by turbulent fluxes (Emeis, 2013). In the Ekman layer an equilibrium is often observed between pressure, Coriolis and frictional forces (Emeis, 2013).

Wind velocity will vary strongly in time at one measurement point, as turbulent eddies pass the measurement station. To get a representative measure of the large-scale velocity field, the flow needs to be averaged over time. The field variable wind velocity can be split into two parts with the use of Reynolds decomposition, one representing the slowly varying mean field (overbars in Eq. (3.7)) and one representing the strongly varying turbulent components (primes in Eq. (3.7)) (Holton, 1992). The mean of the total acceleration of the 3-dimensional flow field can then be rewritten as Eq. (3.8) and in a similar matter for the v and w components. The mean horizontal momentum balance equation is then written as Eqs. (3.9) and (3.10).

$$u = \bar{u} + u' \quad \& \quad v = \bar{v} + v' \quad \& \quad w = \bar{w} + w' \tag{3.7}$$

$$\overline{\frac{Du}{Dt}} = \frac{D\bar{u}}{Dt} + \frac{\partial}{\partial x}(\overline{u'u'}) + \frac{\partial}{\partial y}(\overline{u'v'}) + \frac{\partial}{\partial z}(\overline{u'w'}) \tag{3.8}$$

$$\underbrace{\frac{\partial \bar{u}}{\partial t}}_{acceleration\ term} + \underbrace{\bar{u}\frac{\partial \bar{u}}{\partial x} + \bar{v}\frac{\partial \bar{u}}{\partial y} + \bar{w}\frac{\partial \bar{u}}{\partial z}}_{advection\ terms} = \underbrace{f\bar{v}}_{Coriolis\ term} - \underbrace{\frac{1}{\rho}\frac{\partial \bar{p}}{\partial x}}_{pressure\ term} - \underbrace{\left[\frac{\partial \overline{u'u'}}{\partial x} + \frac{\partial \overline{u'v'}}{\partial y} + \frac{\partial \overline{u'w'}}{\partial z}\right]}_{turbulent\ flux\ term} \tag{3.9}$$

$$\underbrace{\frac{\partial \bar{v}}{\partial t}}_{acceleration\ term} + \underbrace{\bar{u}\frac{\partial \bar{v}}{\partial x} + \bar{v}\frac{\partial \bar{v}}{\partial y} + \bar{w}\frac{\partial \bar{v}}{\partial z}}_{advection\ terms} = \underbrace{-f\bar{u}}_{Coriolis\ term} - \underbrace{\frac{1}{\rho}\frac{\partial \bar{p}}{\partial y}}_{pressure\ term} - \underbrace{\left[\frac{\partial \overline{u'v'}}{\partial x} + \frac{\partial \overline{v'v'}}{\partial y} + \frac{\partial \overline{v'w'}}{\partial z}\right]}_{turbulent\ flux\ term} \tag{3.10}$$

Further simplification of Eqs. (3.9) and (3.10) can be obtained by assuming horizontal homogeneity, i.e. no structures/anomalies on the earth surface, so that horizontal turbulent fluxes are homogeneous (Holton, 1992). This implies that the $\frac{\partial \overline{u'u'}}{\partial x}, \frac{\partial \overline{u'v'}}{\partial y}, \frac{\partial \overline{u'v'}}{\partial x}, \frac{\partial \overline{v'v'}}{\partial y}$ terms in Eqs. (3.9) and (3.10) are very small. A simplified version of the horizontal atmospheric momentum balance in the ABL, neglecting molecular friction and assuming horizontal homogeneity are given by Eqs. (3.11) and (3.12). In this way, the turbulent flux term acts as a damping mechanism for $\frac{Du}{Dt}$ and $\frac{Dv}{Dt}$.

$$\underbrace{\frac{\partial \bar{u}}{\partial t}}_{acceleration\ term} + \underbrace{\bar{u}\frac{\partial \bar{u}}{\partial x} + \bar{v}\frac{\partial \bar{u}}{\partial y} + \bar{w}\frac{\partial \bar{u}}{\partial z}}_{advection\ terms} = \underbrace{f\bar{v}}_{Coriolis\ term} - \underbrace{\frac{1}{\rho}\frac{\partial \bar{p}}{\partial x}}_{pressure\ term} - \underbrace{\frac{\partial \overline{u'w'}}{\partial z}}_{turbulent\ flux} \tag{3.11}$$

$$\underbrace{\frac{\partial \bar{v}}{\partial t}}_{acceleration\ term} + \underbrace{\bar{u}\frac{\partial \bar{v}}{\partial x} + \bar{v}\frac{\partial \bar{v}}{\partial y} + \bar{w}\frac{\partial \bar{v}}{\partial z}}_{advection\ terms} = \underbrace{-f\bar{u}}_{Coriolis\ term} - \underbrace{\frac{1}{\rho}\frac{\partial \bar{p}}{\partial y}}_{pressure\ term} - \underbrace{\frac{\partial \overline{v'w'}}{\partial z}}_{turbulent\ flux} \tag{3.12}$$

3.4 Experimental contribution analysis of the momentum balance

An assessment of the magnitude of the various terms in the momentum balance is performed by Holton (1992) by a scale analysis, as described in section 2.2. This scale analysis is also applicable to the time average horizontal momentum balance Eqs. (3.11) and (3.12), and yields the same results. The total derivative of the 3-dimensional flow field ($\frac{Du}{Dt}$ and $\frac{Dv}{Dt}$), is considered to be of the magnitude 10^{-4} m/s^2 and one order smaller than the pressure and Coriolis term. In the scaling analysis however, $\frac{Du}{Dt}$ and $\frac{Dv}{Dt}$ are not split up in their local acceleration and advection component. Holton (1992) only states that in general the advective terms and local acceleration terms are of comparable magnitudes. Also, the contribution of the turbulent flux term to the momentum balance is unknown by the scaling analysis. This motivates to look at the individual contributions to the momentum balance, with the use of spatially varied observation data.

Chapter 4: Momentum budget

The momentum budget quantifies the contributions of each term in the momentum balance, i.e. the driving forces of the atmospheric flow. In the free atmosphere, above the ABL, the effects of the surface can be neglected and flow is mainly governed by large scale pressure gradients. The momentum balance may therefore be simplified while maintaining sufficient accuracy. As indicated by Holton (1992) and Emeis (2013), the momentum balance of atmospheric flow in the ABL is more complex and involves more physical quantities.

KNMI data on pressure and wind velocity from 48 measurement stations (Appendix) over a two-year period (01/07/2016 t/m 30/05/2018) is used to make a comprehensive analysis of the momentum budget. The data set was initially processed and provided by Pim van Dorp of the weather forecasting company Whiffle. The pressure, pressure gradient, velocity and velocity gradient at the Cabauw measurement station location are determined by a 2-dimensional linear interpolation based on the observations of 48 KNMI measurement stations within a 100-km radius of the Cabauw location. The interpolation method used is known as "the Bosveld method" named after Fred Bosveld of the KNMI. With the 2-year data set, it is possible to quantify all relevant terms of the horizontal momentum balance, except the turbulent flux term ($\frac{\partial \overline{u'w'}}{\partial z}$ and $\frac{\partial \overline{v'w'}}{\partial z}$). However, the turbulent flux can be derived as the residual of the momentum balance. The validity of the turbulent flux term is somewhat uncertain as all measurement errors and uncertainties of the other physical quantities propagate into the turbulent flux term. As the measurements on pressure, pressure gradient, velocity and velocity gradient are relatively simple and therefore made with sufficient accuracy, the results on the residual are representative for the true turbulent flux term. The following analysis of the momentum balance and its components is based on this data set.

4.1 Turbulent fluxes

Above the turbulent atmospheric layer, the momentum dynamics can be simplified by quantifying some contributions in the momentum balance as negligible. For synoptic-scale phenomena only the acceleration, pressure gradient and Coriolis term are considered. The scale analysis by Holton (1992) implied that the total acceleration terms is of one magnitude smaller than the pressure term and Coriolis term. Also, in case there is no net acceleration, the wind is governed by the Geostrophic flow equation. This would mean that the pressure term and Coriolis term are opposite but of the same magnitude, and follow a 1:1 relation. A scatter plot of the pressure term and Coriolis term (Figure 3) shows strong bias towards the pressure term. The plot shows that the Coriolis term has a magnitude of only a third of the pressure term in both the u and v component. An imbalance between the pressure gradient driven force and Coriolis force, results in a very strong wind acceleration if no other physical quantities would influence the balance. The resulting magnitude of acceleration seems too large, and motivates to look at other terms in the momentum balance that would act as a damping force to this acceleration.

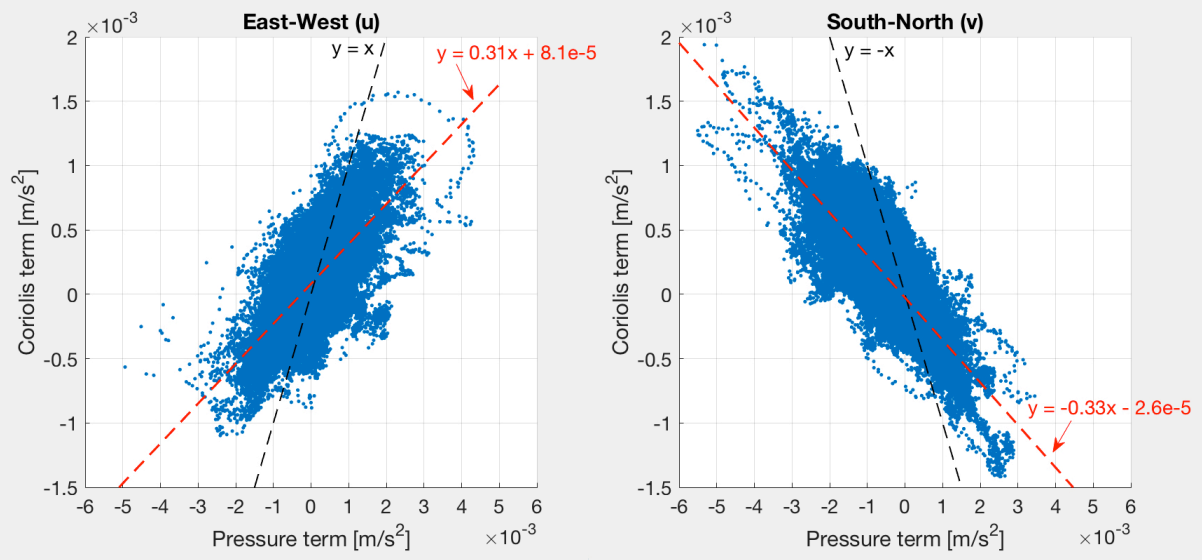

Figure 3: Scatter plot of Pressure term and Coriolis term for wind velocity components East-West (u) and South-North (v). For velocity component East-West (u): pressure = $\frac{1}{\rho}\frac{\partial \bar{p}}{\partial x}$, Coriolis = $f\bar{v}$ and South-North (v): pressure = $\frac{1}{\rho}\frac{\partial \bar{p}}{\partial y}$, Coriolis = $-f\bar{u}$. Data by KNMI observation stations and processed by Whiffle. Period: 01/07/2016 – 30/05/2018.

If only pressure gradient and Coriolis force are the driving forces of acceleration, their difference, known as the geostrophic wind acceleration $f(v - v_{geo})$ and $f(u - u_{geo})$, would balance with the total acceleration $(\frac{Du}{Dt})$ and $(\frac{Dv}{Dt})$ in the total momentum budget. In Figure 4 a scatter plot is presented of the acceleration term due to the imbalance between the Coriolis and pressure gradient forces, which we define as ageostrophic acceleration, and total acceleration. The weak correlation between ageostrophic and total acceleration implies that there is no bulk balance between the total acceleration, Coriolis and pressure gradient forces. The residual of this imbalance must be equal to a damping force working on the momentum balance. Although Figure 4 shows a weak correlation of ageostrophic acceleration with the total acceleration of the flow field, it is clear that a damping force plays an even so important but opposite role in the momentum balance.

According to the momentum balance as in Eqs. (3.11) and (3.12) the turbulent flux term acts as this damping force to the complete acceleration budget. Together with the findings from Figures 3 and 4, it is apparent that turbulent motion in the ABL acts as a break on the acceleration force induced by the imbalance of the pressure term and Coriolis term. The magnitude of the turbulent flux term is of the same order as the pressure and Coriolis term, and therefore cannot be neglected in the momentum balance of the ABL.

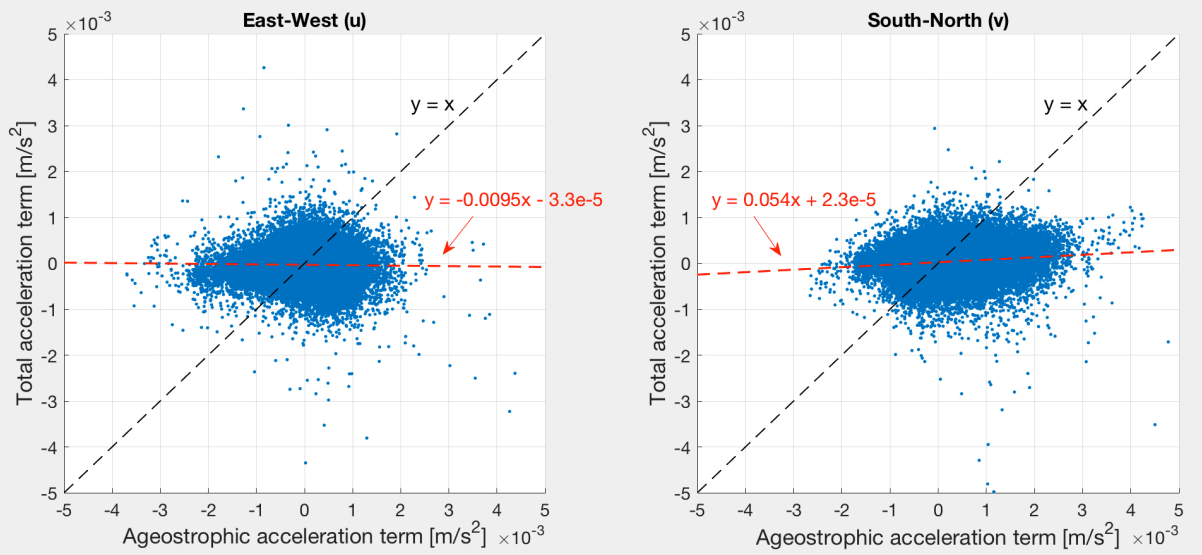

Figure 4: Scatter plot of Ageostrophic acceleration term and Total acceleration term for wind velocity components East-West (u) and South-North (v). Data by KNMI observation stations and processed by Whiffle. Period: 01/07/2016 – 30/05/2018.

4.2 Parameterization of turbulent fluxes

When the atmosphere is built up out of a convective boundary layer with a stable layer on top, turbulent mixing will result in the formation of a well-mixed layer. Such well-mixed layers are formed over land on cloud free days when surface heating is strong (Holton, 1992). In these well mixed-boundary layers, wind velocity and temperature are almost independent of elevation (Holton, 1992). For this reason, the layer may be treated as one slab with temperature and wind speed constant with height, so that turbulent fluxes vary linearly with elevation. Turbulent momentum fluxes can then be defined by Eq. (4.1), known as the bulk aerodynamic formula (Holton, 1992). This parameterization can also be used for night-time when the boundary layer is not well mixed, differences in layer conditions are translated in parameter C_d.

$$\overline{u'w'} = -C_d|\bar{V}|\bar{u} \qquad \overline{v'w'} = -C_d|\bar{V}|\bar{v} \tag{4.1}$$

In the Bulk Aerodynamic Eq. (4.1), C_d is the non-dimensional drag coefficient and $|\bar{V}| = \sqrt{(\bar{u}^2 + \bar{v}^2}$ is the absolute wind velocity. According to literature C_d over water is in the order of $1.5\text{x}10^{-3}$, but may be several times larger over land and rough surfaces (Holton, 1992). The momentum balance applicable to the ABL Eqs. (3.11) and (3.12) can be integrated over height from the surface to the top of the ABL at z = h. This yields in a form of the bulk aerodynamic formula over the full atmospheric column Eq. (4.2). The parameters defining the relation between turbulent flux and velocity can be lumped together as in Eq. (4.3) and be defined as coefficient K.

$$\frac{\overline{u'w'}}{h} = \frac{-C_d|\bar{V}|\bar{u}}{h} \qquad \frac{\overline{v'w'}}{h} = \frac{-C_d|\bar{V}|\bar{v}}{h} \tag{4.2}$$

$$\frac{\overline{u'w'}}{h} = -K\bar{u} \qquad \frac{\overline{v'w'}}{h} = -K\bar{v} \tag{4.2}$$

It is now interesting to see if we can find a linear relation between velocity and turbulent flux in the 2-year observation data, and quantify the coefficient K. A scatter plot of the turbulent flux acceleration and the wind velocity (Figure 5), shows the expected linear relation. The data set is split up into day time and night time turbulent fluxes, and a small difference in correlation coefficient K is evident. Night-time: $K_u = -1.4 \times 10^{-4}\ s^{-1}$, $K_v = -2.2 \times 10^{-4}\ s^{-1}$ and for day-time: $K_u = -1.2 \times 10^{-4}\ s^{-1}$, $K_v = -1.8 \times 10^{-4}\ s^{-1}$. Reasons for a larger night-time K, than K for day-time may include stronger turbulence and larger depth of the ABL at day time. An elaboration on stronger turbulence during day-time is given in section 4.3. Also, the coefficient K is larger for the v component of the wind velocity. The strong relation between turbulent flux term and velocity term gives confidence that turbulence plays an important role in the complete momentum budget.

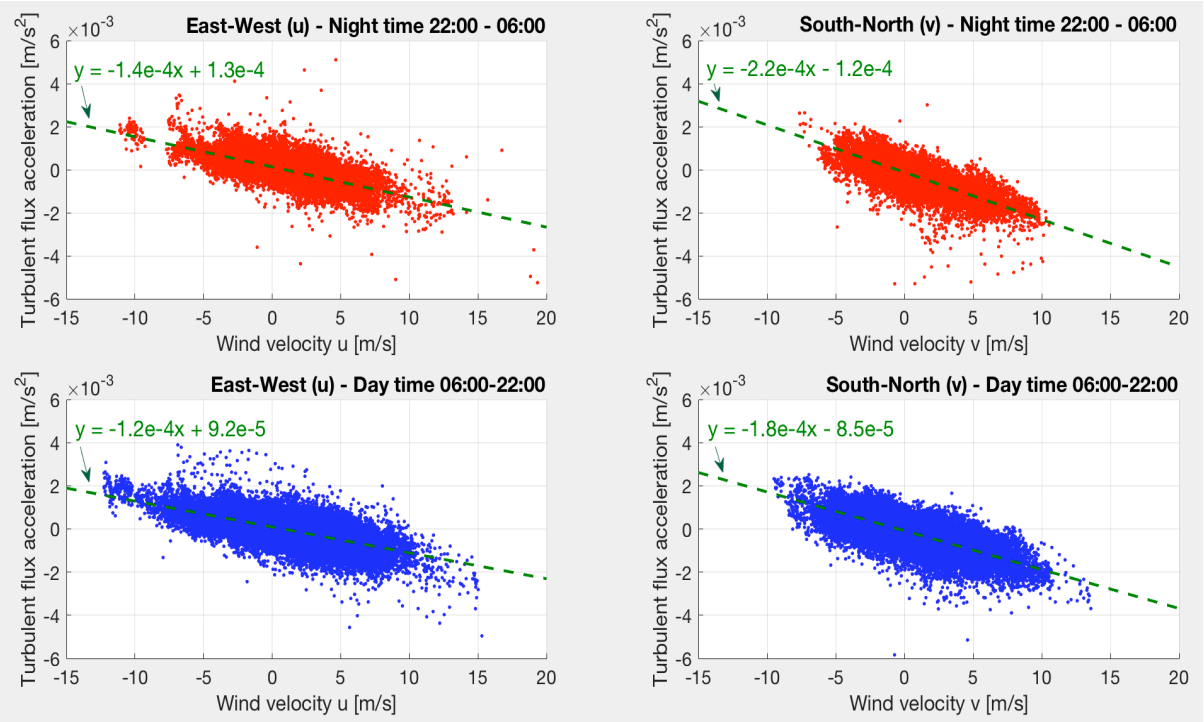

Figure 5: Scatter plot of the diagnosed turbulent flux term and wind velocity for components u and v, split in day-time and night-time. The RMS line represents a linear regression between the turbulent flux and velocity term. Data by KNMI observation stations and processed by Whiffle. Period: 01/07/2016 – 30/05/2018, Time: Local time at Cabauw.

4.3 Diurnal cycle

According to Emeis (2013) strong diurnal variation in wind speed occurs, with higher velocities at night and lower velocities during the day. Also, this diurnal variation is a function of elevation, with stronger variations at higher elevations and weaker variations at lower elevations. A wind velocity analysis by de Roode at the Cabauw site shows that the wind velocity at night is larger than during the day above 20 meters elevation. Below 20 meters elevation the wind velocity at night is smaller than during the day. As apparent from the previous analysis, turbulence has a strong influence on the ABL momentum balance, and it is known that the magnitude of turbulence varies between night and day (Vila-Guerau de Arellano, n.d.). The turbulence responsible for the diurnal wind velocity dynamics can be split up into the forcing by convective turbulence and by mechanical turbulence. For the diurnal changes, the convective turbulence is of main importance, but mechanical turbulence can significantly contribute, e.g. the enhanced growth of ABL during morning transition (Vila-Guerau de Arellano, n.d.).

To see if we are able detect a diurnal cycle in the turbulent flux term from the observations, it is interesting to look at a period of days where the total turbulent budget is well understood. This is the case for a continuous period in which no clouds are present in the observation domain. This weather type occurs in the presence of a persisting high-pressure system resulting in a repetition of the diurnal weather cycle, with strong convection during the day and vanishing or weak turbulence during the night. A case study is presented for the period: 3/5/2018 up to and including 7/5/2018. Night and day time are set to sunrise and sunset for that period, hence 05:20-20:00 local time at Cabauw for day-time and 20:00-05:20 local time at Cabauw for night-time. The complete momentum budget for this period on a 10-minute interval is presented in Figure 6. This representation shows that the Coriolis term and pressure term often almost fully counteract each other, but not always. For some periods, the pressure term and Coriolis term are of the same magnitude, however for other periods the previous described bias in magnitude demonstrates itself. Figure 6 shows that this imbalance is mainly damped by the turbulent flux term. The acceleration caused by turbulence is either positive or negative, but counter acting the acceleration induced by the imbalance of the pressure gradient force and Coriolis force. The sign is therefore dependent upon the direction of flow.

According to the observations on the cloud free day, the advective acceleration and local acceleration are about one magnitude smaller (10^{-4}) than the Coriolis and pressure term (10^{-3}). This is in accordance with the scale analysis of Holton (1992), and as apparent also applicable to the ABL. For short periods, i.e. a few hours, the local acceleration and advective acceleration are of the same sign or opposite sign and change often. This continuous change in acceleration and deceleration on a small-time interval, hints to the large velocity gradient observations made in Figure 1.

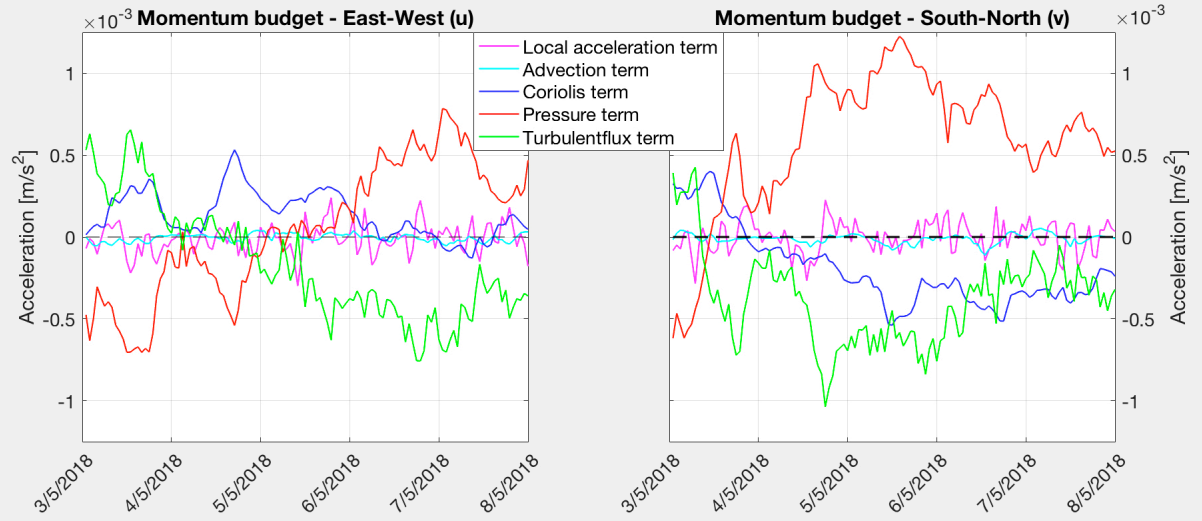

Figure 6: Momentum budget of velocity components u and v for cloud free period: 03/05/2018 - 07/05/2018. Data by KNMI observation stations and processed by Whiffle.

The magnitude of acceleration caused by the turbulent flux over this period is presented for a 10-minute interval (Figure 7). This plot clearly shows that during day time (blue) the turbulent flux acceleration is of larger magnitude compared to night time (red) turbulent flux acceleration. The diurnal repeating trend is evident for both flow direction components, but more profound for the South-North component resulting from the orientation of the pressure field in this case study (Figure 7). Also, the day time turbulent flux term has a larger variance compared to night time flux. At night, the turbulent flux seems to be more stable with a smaller spread in acceleration. The diurnal turbulence increases and decreases plus difference in variance is not only restricted to cloud free days. The pattern is also detectible in other periods with different weather types, however most profound on cloud free days.

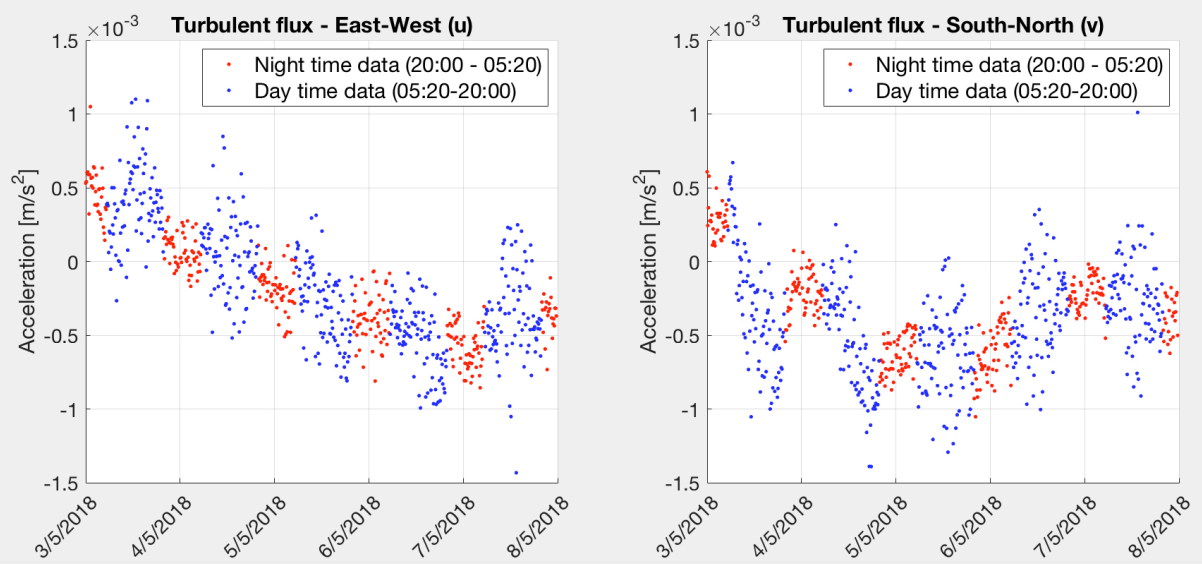

Figure 7: Turbulent flux term on 10-minute interval of velocity components u and v for day-time and night-time of a period of cloud free days. Data by KNMI observation stations and processed by Whiffle. Period: 03/05/2018 - 07/05/2018, Time: Local time at Cabauw.

4.4 Mean momentum budget

The KNMI observation data can also be used to diagnose the annual mean horizontal momentum budget. In Figure 8 a representation is given of the absolute mean contribution of each acceleration term to the momentum balance. The ageostrophic acceleration is comprised of imbalance between the pressure term and Coriolis term and presents the deviation of the geostrophic win. Also in this budget, it is clear that the turbulent flux term counteracts the imbalance of the pressure and Coriolis term, as they take up about the same fraction of the momentum budget.

For the East-West (u) velocity component, the mean turbulent flux is smaller during night-time than during day-time. This is comparable with the day-time and night-time turbulence analysis in section 4.3. Note that although during night-time the mean magnitude of the turbulent flux is smaller than during day-time, the fraction it takes up of the momentum budget is slightly larger at night-time compared to day-time. However, for the South-North (v) velocity component, the mean turbulent flux is larger during night-time than during day-time. Note that this is not similar with the day-time and night-time turbulence analysis on a period of stable, clear sky weather in section 4.3. A 2-year mean 24-hour turbulent flux budget for the u and v velocity components is presented in the Appendix. Various weather types have different effects on turbulence during night and day, the 2-year mean diurnal turbulent flux budget (Figure A1) can therefore not be compared to the diurnal turbulent flux budget over a clear sky period. However, the discrepancy in diurnal turbulent flux variation for the velocity components u and v, motivates to further investigate the day and night turbulent flux variation and turbulent flux variation for different weather systems in future research.

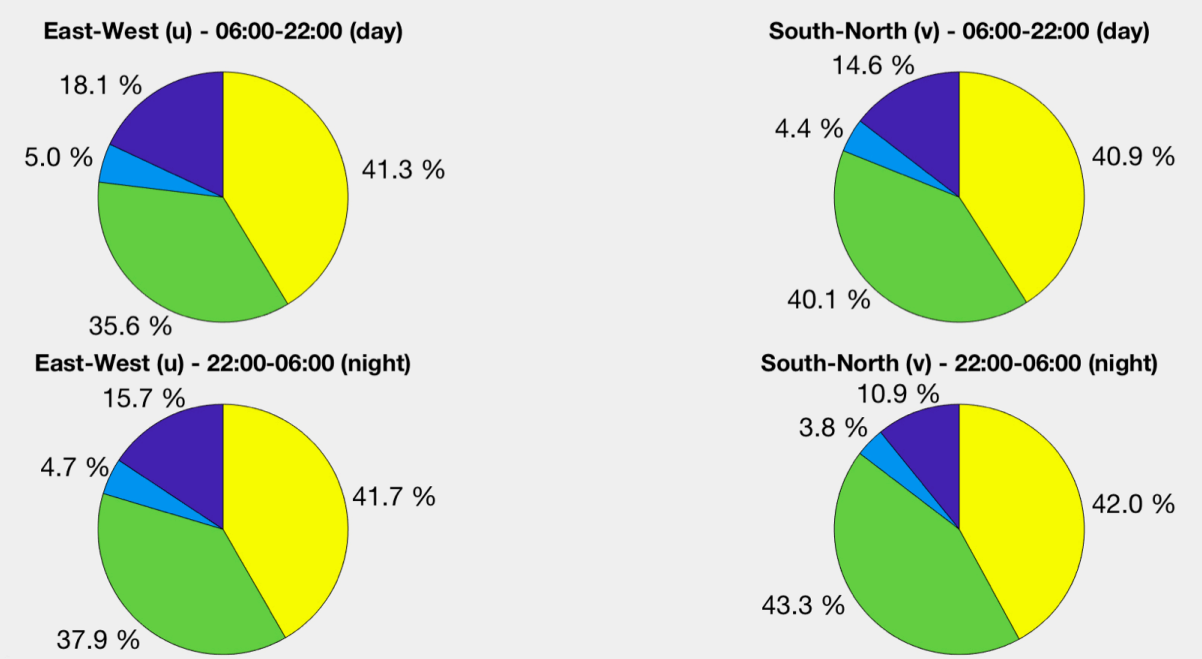

Term	Color	(u) day [m/s2]	(u) night [m/s2]	(v) day [m/s2]	(v) night [m/s2]
Local Acceleration		2.13e-04	1.71e-04	2.09e-04	1.65e-04
Advection		5.93e-05	5.10e-05	6.24e-05	5.78e-05
Ageostrophic Acceleration		4.20e-04	4.13e-04	5.74e-04	6.60e-04
Turbulent flux		4.88e-04	4.53e-04	5.86e-04	6.41e-04

Figure 8: Mean momentum budget according to Eqs. (3.11) and (3.12) for wind velocity components u and v, split up in day-time and night-time. Data by KNMI observation stations and processed by Whiffle. Period: 01/07/2016 – 30/05/2018, Time: Local time at Cabauw.

Conclusion

Based on 2-year observation data of 48 KNMI measurement stations in a 100-km radius of Cabauw it is apparent that the pressure and Coriolis gradient forces strongly deviate from the geostrophic balance. It is found that the Coriolis term in the momentum balance has a magnitude of only a third of the pressure term. The weak correlation between ageostrophic and total acceleration implies that there is no bulk balance between the total acceleration, Coriolis and pressure gradient forces. The turbulent flux term was diagnosed as a residual from the horizontal momentum balance. The imbalance between pressure and Coriolis is countered by turbulence, which has the same order of magnitude as the pressure term and acts as a damping force to flow acceleration. Analysis shows that turbulent fluxes vary linearly with wind velocity and the coefficient K for this relation can be quantified and varies slightly between night and day. Diurnal trends in the momentum balance and especially of turbulence are diagnosed for a period of stable, clear sky weather. The results herein show that turbulent fluxes are stronger and have a larger variance during day-time compared to night-time. In addition, the 2-year mean momentum budget shows that acceleration by turbulent friction takes up the same fraction as the ageostrophic acceleration in the total momentum balance. So, for turbulent layers, i.e. the Atmospheric Boundary Layer, turbulence is of significant importance and cannot be neglected in the horizontal momentum balance.

Reference

Apxgroup.com. (2018). EPEX SPOT | Welcome |. [online] Available at: https://www.apxgroup.com [Accessed 30 May 2018].

Emeis, S. (2013). Wind Energy Meteorology. 1st ed. Berlin, Heidelberg: Springer, pp.2-30.

Holton, J. (1992). An introduction to dynamic meteorology. 3rd ed. San Diego: Academic Press, pp.1-138.

van der Hurk, B., van Meijgaard, E., & Lenderink, G. (2018). Update on the KNMI Regional Climate Model RACMO (pp. 1-12). Retrieved from http://www.climatechangesspatialplanning.nl/media/default.aspx/emma/org/10354124/6-12+Update+on+the+KNMI+Regional+Climate+Model+RACMO.pdf

Knmi.nl. (2018). KNMI - Meetmast Cabauw. [online] Available at: https://www.knmi.nl/kennis-en-datacentrum/uitleg/meetmast-cabauw [Accessed 31 May 2018].

Kurien, S. and Taylor, M. (2005). Direct Numerical Simulations of Turbulence. Los Alamos Science, [online] 29, pp.142 - 150. Available at: https://pdfs.semanticscholar.org/56fb/7a5727eeb25f2762dcdf41270b7fcf2b641b.pdf [Accessed 30 May 2018].

J. H. LaCasce, J. (2008). A Brief Introduction to Atmospheric Dynamics. [ebook] Oslo. Available at: http://www.uio.no/studier/emner/matnat/geofag/GEF4500/h08/unisdyn1.pdf [Accessed 28 May 2018].

Mesoscale Research Group (2014). Synoptic Meteorology I: The Geostrophic Approximation. [ebook] pp.1-12. Available at: http://derecho.math.uwm.edu/classes/SynI/GeosApprox.pdf [Accessed 31 May 2018].

Nilsson, E., Sahlée, E. and Rutgersson, A. (2013). Turbulent momentum flux characterization using extended multiresolution analysis. Quarterly Journal of the Royal Meteorological Society, 140(682), pp.1715-1728.

Qian, W. (2017). Temporal Climatology and Anomalous Weather Analysis. Singapore: Springer Singapore.

de Roode, S. R., Frederikse, T., Siebesma, A., Ackerman, A., Field, P., Hill, A., Fricke, J., Gryschka, M., Honnert, R., Lac, C., Krueger, S., Lesage, A. and Tomassini, L. (n.d.). Turbulent transport in the Grey Zone: A large-eddy simulation model intercomparison study of the CONSTRAIN cold air outbreak case. To be submitted to: Journal of Advances in Modeling Earth Systems (JAMES).

Schalkwijk, J., Jonker, H., Siebesma, A. and Bosveld, F. (2015). A Year-Long Large-Eddy Simulation of the Weather over Cabauw: An Overview. Monthly Weather Review, 143(3), pp.828-844.

Strikwerda, J. (2004). Finite difference schemes and partial differential equations. Philadelphia: Society for Industrial and Applied Mathematics, pp.165-170.

U.S. Department of Energy (2015). Wind vision. [image] Available at: https://www.energy.gov/sites/prod/files/wv_chapter3_impacts_of_the_wind_vision.pdf [Accessed 25 Jun. 2018].

USNA (n.d.). Lesson 6: Geostrophic, Thermal and Gradient Winds. [ebook] Available at: https://www.usna.edu/Users/oceano/barrett/SO513/Lesson6_Geostrophy_thermal_gradient_winds.docx Lesson 6: Geostrophic, Thermal and Gradient Winds [Accessed 31 May 2018].

Valero-Lara, P. (2018). Analysis and Applications of Lattice Boltzmann Simulations. Hershey: IGI Global, p.339.

Vila-Guerau de Arellano, J. (n.d.). Atmospheric boundary layer. 1st ed. Cambridge University Press, pp.62-84.

Appendix

List of 48 used KNMI metrological measurement stations within 100 km radius of the Cabauw station:

"D15-FA-1", "P11-B", "K14-FA-1C", "A12-CPP", "F16-A", "L9-FF-1",
"AWG-1", "J6-A", "HOORN-A", "BUITENGAATS/BG-OHVS2", "VOORSCHOTEN AWS",
"IJMUIDEN WP", "DE KOOIJ VK", "F3-FB-1", "AMSTERDAM/SCHIPHOL AP",
"VLIELAND", "WIJDENES WP", "BERKHOUT AWS", "TERSCHELLING HOORN AWS",
"WIJK AAN ZEE AWS", "HOUTRIBDIJK WP", "DE BILT AWS", "STAVOREN AWS",
"LELYSTAD AP", "LEEUWARDEN", "MARKNESSE AWS", "DEELEN", "LAUWERSOOG AWS",
"HEINO AWS", "HOOGEVEEN AWS", "GRONINGEN AP EELDE", "HUPSEL AWS",
"NIEUW BEERTA AWS", "TWENTE AWS", "VLISSINGEN AWS", "WESTDORPE AWS",
"HOEK VAN HOLLAND AWS", "WOENSDRECHT", "ROTTERDAM GEULHAVEN",
"ROTTERDAM THE HAGUE AP", "CABAUW TOWER AWS", "GILZE RIJEN",
"HERWIJNEN AWS", "EINDHOVEN AP", "VOLKEL", "ELL AWS",
"MAASTRICHT AACHEN AP", "ARCEN AWS"

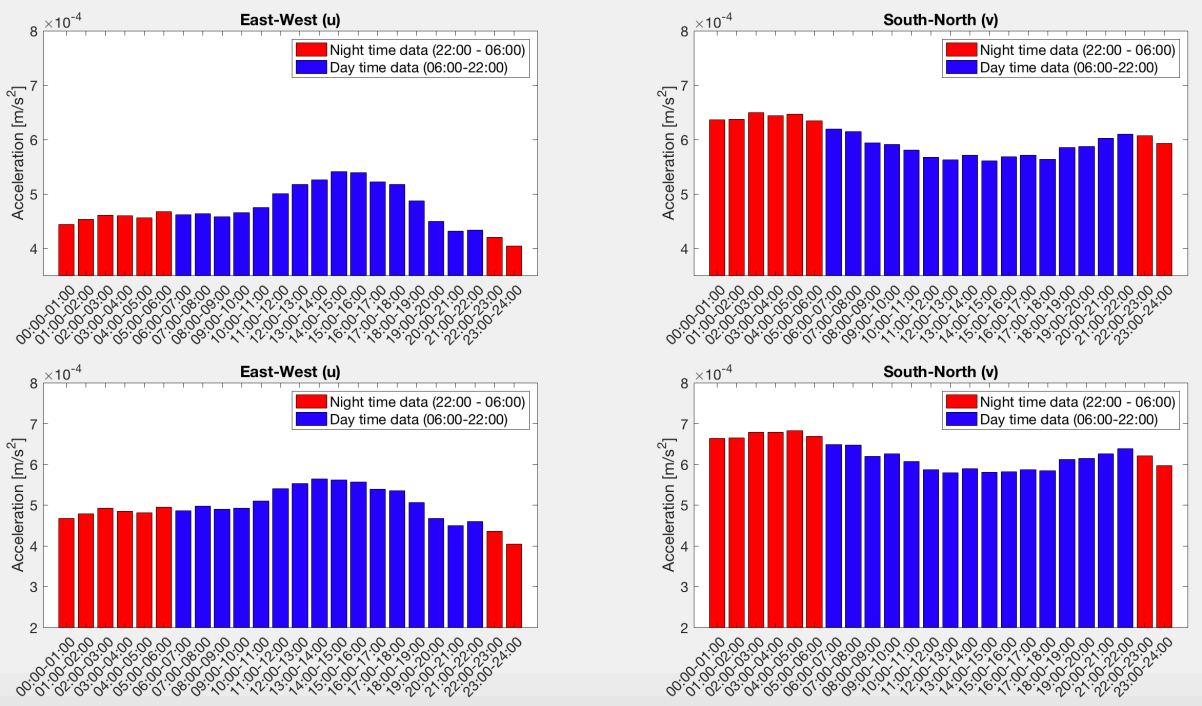

Figure A1: Diurnal variation in acceleration of the wind velocity due to turbulent friction, this term was diagnosed as a residual from the horizontal momentum balance. Wind velocity components u and v, split in an indicative day-time and night-time set. True day and night time vary between seasons. Data by KNMI observation stations and processed by Whiffle. Period: 01/07/2016 – 30/05/2018, Time: Local time at Cabauw.